Submitted to Applied Optics

LBL-3140
Preprint c. 2

REFLECTION EFFECTS IN INTERFEROMETRY

F. R. McLarnon, R. H. Muller, and C. W. Tobias

April 1975

Prepared for the U. S. Energy Research and Development Administration under Contract W-7405-ENG-48

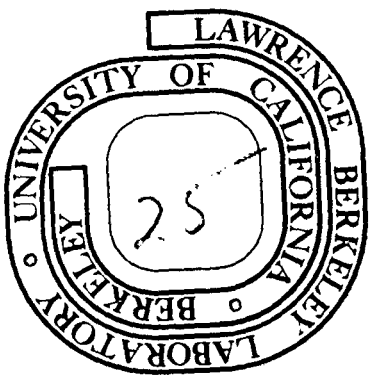

DISCLAIMER

LBL-3140

REFLECTION EFFECTS IN INTERFEROMETRY

F. R. McLarnon, R. H. Muller and C. W. Tobias

Inorganic Materials Research Division, Lawrence Berkeley Laboratory and
Department of Chemical Engineering; University of California
Berkeley, California 94720

ABSTRACT

Spurious distortions of interference fringes are often encountered in the interferometry of planar solid-fluid phase boundaries. These distortions mimic refractive-index variations near the interface and introduce uncertainty in locating the position of the interface on the interferogram. Light reflection from the slightly rounded edge of the solid surface has been identified as the principal cause of these distortions.

INTRODUCTION

Interferometry has been frequently used for the observation of refractive-index variations in fluids near solid surfaces.[1-3] When no refractive-index gradients are present in the interfacial region, i.e., the fluid has everywhere a constant refractive-index, interference fringes that are oriented normal to the interface are expected to be straight up to the solid surface, and the solid-fluid interface is expected to coincide with the shadow of the solid on the interferogram. However, spurious fringe displacements in the interferograms of solid-fluid phase boundaries are often observed. We have now identified reflection as the chief cause of these distortions; the interference fringes bend as if a refractive-index gradient existed near the interface. Another limitation in the optical observation of such phase boundaries is diffraction, which will not be considered here.

Because reflected rays will traverse the fluid along jointed lines (unreflected rays traverse a homogeneous fluid along straight lines), two types of distortions result in the interferogram: (a) Geometrical distortion due to displacement of the beam normal to its original propagation direction. This effect falsifies conventional interpretation of distance on the interferogram and causes displacement of the apparent interfacial location. (b) Phase distortion due to increased geometrical path length. The magnitude and character of each of these abberations depend strongly[4] on the choice of the plane of focus of the imaging objective lens.

It is the purpose of this paper to present sample calculations of interferogram distortions caused by reflection from the slightly

rounded edge at the light-entrance side of an otherwise planar surface and compare them with the corresponding experimental results. We also propose two simple methods for minimizing such reflection effects.

REFLECTION FROM THE ROUNDED EDGE OF A PLANAR SURFACE

Figure 1 schematically illustrates the reflection of a ray ABC from the rounded edge of a plane surface $y = 0$ at point B. According to the Law of Reflection, the angle CBE, with respect to the surface tangent plane DBE, equals the angle ABD. Rays that enter the specimen at ordinates above the planar region of the solid ($y \geqslant 0$) will not reflect from the surface and will traverse the specimen along straight lines parallel to the plane $y = 0$.

Figure 2 illustrates the trajectory of a reflected ray ABCD as it traverses a specimen consisting of a homogeneous fluid layer above a solid, both bounded by parallel flat glass sidewalls. The light ray is incident perpendicular to the glass walls and parallel to the planar region $y = 0$ of the solid surface.

Application of the Law of Reflection at point B in Fig. 2 provides the angle ϕ_f of the reflected ray $x_B \leqslant x \leqslant w$. The angle ϕ_g of the ray in the glass wall ($w \leqslant x \leqslant w + d$) is easily calculated from Snell's Law,

$$n_f \cdot \sin\phi_f = n_g \cdot \sin\phi_g \quad , \tag{1}$$

and geometrical considerations show that the ray leaves the specimen at

$$y_D = y_B + (w - x_B) \cdot \tan\phi_f + d \cdot \tan\phi_g \quad . \tag{2}$$

The beam has thus been displaced from its original location $y = y_B$ at $x = 0$ to $y = y_D$ at $x = w + D$. At the latter plane the ray enters the

surrounding medium (e.g., air) and propagates to the interferometer imaging optics at an angle ϕ_a, easily calculated by Snell's Law. The optical path length p_r of reflected ray ABCD is given by

$$p_r = n_f \cdot x_B + n_f \cdot (w - x_B) \sqrt{1 + \tan^2\phi_f} + n_g \cdot d \sqrt{1 + \tan^2\phi_g} \quad . \quad (3)$$

All rays, provided they are accepted by the objective lens of the interferometer, appear to emanate from the virtual plane of focus QR of the objective lens. The virtual plane of focus is calculated[4] from the real plane of focus (which is optically conjugate to the interferometer film plane) as follows: If the real plane of focus lies at some plane $x = x_f$, the virtual plane of focus lies at the plane $x = w + d - F$, where

$$F = \frac{w - x_f}{n_f} + \frac{d}{n_g} \quad . \quad (4)$$

F is depicted on Fig. 2 as the horizontal distance between the plane of light-exit from the specimen and the virtual plane of focus RQ.

The reflected ray ABCD on Fig. 2 appears to emanate from its virtual origin Q, which is a vertical distance $S = F \cdot \tan\phi_a$ below the location Y_D where the reflected ray leaves the specimen. Therefore, the reflected ray ABCD appears on the interferogram at a position

$$y_i = y_D - F \cdot \tan\phi_a \quad . \quad (5)$$

The phase on the interferogram is calculated by comparing the optical path of the reflected ray Eq. (3) with that of a hypothetical unreflected ray GQE passing through the virtual origin Q with the space between the glass walls filled with liquid. The exit points D and E of each ray lie on an equiphase arc DE centered on the virtual origin Q.

The exit points D and E of each ray lie on an equiphase arc DE centered on the virtual origin Q. Beyond points D and E the interferometer introduces no phase difference between the rays ABCD and GQE. The optical path p_o of the hypothetical unreflected ray GQE is calculated by considering the length $T = F\left(\sqrt{1 + \tan^2\phi_a} - 1\right)$:

$$p_o = n_f \cdot w + n_g \cdot d + n_a \cdot F \cdot \left(\sqrt{1 + \tan^2\phi_a} - 1\right) \tag{6}$$

The phase on the interferogram is given in fringe shifts as

$$N = \frac{p_r - p_o}{\lambda} \quad . \tag{7}$$

CALCULATION OF INTERFEROGRAMS FOR REFLECTION FROM THE EDGE OF A PLANAR SURFACE

The present work arises from the interferometric study[4-6] of concentration profiles in aqueous $CuSO_4$ electrolyte near planar copper surfaces. The copper electrodes were w = 10.0 mm wide and fully occupied the space between the d = 12.7 mm wide parallel optically flat glass sidewalls (as in Fig. 2). The traveling, doubly-emitting laser interferometer has been described elsewhere.[5] The objective lens of this interferometer can accept light emanating from the specimen at angles up to 7.0°.

The electrode surfaces were carefully polished with kerosene as a carrier, using progressively finer (up to #600) grades of carbide paper, chromium oxide (initial) and 1 μm diamond paste (final) abrasives. Electrode surface profiles[7] are illustrated in Figs. 3 and 4. Figure 3, curve a, represents a typical surface profile for a long (100 cm) electrode, Fig. 4, curve a, shows the most square

surface that could be obtained for a short (5 cm) electrode, and Fig. 4, curve b, indicates a surface with a deliberately rounded edge. The actual surface roughnesses, not shown on the surface profiles, are about 1.0 μm peak-to-peak. The central (1 mm < x < 9 mm) regions of the surfaces are flat to within 1.0 μm.

The rounded edge shown in Fig. 3, curve a, has been approximated by a hyperbolic curve,

$$y = -0.00125/x \quad , \tag{8}$$

for ease of computation (curve b in Fig. 3).

In the calculations that follow, all incident light rays are assumed to enter the specimen parallel to the planar solid surface y = 0. If the beam entered at a negative angle with respect to the plane y = 0, i.e., impinging on the planar region of the surface, the interferogram distortions due to a reflection would be more pronounced. If the incident rays entered at a positive angle, i.e., the planar part of the surface was shielded by the edge, the distortions would be less pronounced.

The light wavelength used in the calculations was λ = 632.8 nm, corresponding to the HeNe laser light source used in our experiments. The fluid refractive-indices were set as n_f = 1.0 and 1.334, corresponding to air and 0.1 M $CuSO_4$, respectively. The 12.7 mm wide glass sidewalls had a refractive-index n_g = 1.5231. Refraction in the glass walls has a negligible effect[2] on the computed interferogram. The refractive-index of the surrounding medium was set n_a = 1.0 (air).

Calculation of the trajectories and optical paths of several (e.g., 10) reflected rays for different planes of focus allows construction of the interferograms--phase vs distance relationships--associated with reflection from the electrode edge. The following stipulation applies to the calculations: a reflected ray must be accepted by the aperture of the objective lens in order to contribute to the interferogram. Rays emanating from the specimen at angles higher than 7.0° are, therefore, not considered in the construction of the interferogram.

Computed interference fringes are shown in Fig. 5 for different planes of focus. The shape of the curves is seen to depend strongly on the choice of plane of focus (as had been previously found to be the case for interferograms of refractive-index fields[2,4]) and only weakly on the fluid refractive-index. The end point of each curve (e.g., y = -0.03 mm and N = -3 fringes for focus B) is determined by the maximum angle of acceptance of the objective lens (here 7.0°). For a large acceptance angle the curves would extend more, i.e., to lower y-values for focus A and B and to higher y-values for focus C and D. For focus at $x \leq 0$ the interface will thus appear receded from its true location y = 0, and spurious fringe shifts will appear near the apparent interface. These spurious fringes create the false impression that a region of lower refractive-index exists near the apparent interface.

For focus at $x > 0$ the calculations suggest a double value of phase in the interferogram and no distortion in the apparent interfacial location. Therefore, the true interface can be found on the interferogram by choosing a plane of focus $x_f > 0$.

OBSERVED INTERFEROGRAMS

Figure 6 shows experimental interferograms of the interface between homogeneous 0.1 M $CuSO_4$ electrolyte (fluid phase refractive-index corresponds to the dashed lines in Fig. 5) and the edge of the electrode surface as shown by curve a in Fig. 3. Note that there are no concentration or temperature gradients in the electrolyte. For focus at $x \leqslant 0$ the experimental interferograms Fig. 6A and B show substantial agreement with the interference fringes predicted (Fig. 5A and B) for the hyperbolic edge approximation Eq. (8). For focus at $x > 0$ the apparent interface does indeed coincide with the true surface $y = 0$, but the computed double-value of phase cannot easily be identified on the interferogram. Instead, diffraction fringes, caused by defocusing of the "edge" of the electrode surface, appear to be more prominent.

Figure 7 illustrates the effect of the degree of edge-rounding on interferograms of the interfaces between air and the two copper surfaces with edges shown in Fig. 4. With a given plane of focus, the purposely rounded edge produces more distortion on the interferograms (Fig. 7B and D) than the more square edge (Fig. 7A and C).

Figure 8 illustrates the effect of the acceptance angle of the objective lens on the interferogram of the phase boundary between 0.1 M $CuSO_4$ and the copper surface with edge shown in Fig. 3, curve a. A change in the lens aperture from full (7.0°) to restricted (0.5°) acceptance reduces the interferogram distortion (at the expense of geometrial resolution).

DISCUSSION

Figure 6 demonstrates that reflected rays from the even slightly rounded edge of an otherwise planar surface can cause a large discrepancy between the true location of the interface and the apparent location (shadow) in the interferogram. There are two simple methods for finding the true interface when reflection effects are present:

(a) Variation of the plane of focus by moving the camera parallel to the electrode surface until the location does not change with further change in the plane of focus. This technique should not be used when refractive-index gradients are present in the fluid because variations in the plane of focus can have large effects on interferograms.[4]

(b) Restriction of the objective lens aperture so that no off-axis reflected rays are accepted by the lens; as in Fig. 8. As with (a) above, this technique should not be used when refractive-index gradients are present in the fluid. A restriction of the objective lens operture would prevent rays deflected[1,4,6] by the refractive-index field from reaching the camera, causing a loss of optical information on the interferogram.

The effect of edge curvature on the interferograms, shown in Fig. 7, suggests that reflection from macroscopically curved surfaces, i.e., spheres and cylinders, would also distort interferograms. Failure to account for reflection effects in the interferometric study of fluid-phase refractive-index variations near <u>any</u> extended surface can lead to significant errors in the determination of the interfacial location

and interfacial refractive-index. In the interferometry of concentration boundary layers at solid-fluid interfaces, erroneous interfacial concentration and boundary layer thickness would be derived.

ACKNOWLEDGEMENT

This work was done under the auspices of the U. S. Energy Research and Development Administration.

REFERENCES

1. W. Hauf and U. Grigull in Advances in Heat Transfer, J. P. Hartnett and T. F. Irvine, eds. (Academic Press, N. Y., 1970), Vol. 6, pp. 133-366.

2. R. H. Muller in Advances in Electrochemistry and Electrochemical Engineering, R. H. Muller, ed. (Wiley-Interscience, N. Y., 1973), Vol. 9, pp. 326-353.

3. R. B. Kennard, J. Res. Natl. Bur. Stand. (U. S.) 8, 787 (1932).

4. K. W. Beach, R. H. Muller and C. W. Tobias, J. Opt. Soc. Am. 63 559 (1973).

5. K. W. Beach, R. H. Muller and C. W. Tobias, Rev. Sci. Instr. 40, 1248 (1969).

6. F. R. McLarnon, R. H. Muller and C. W. Tobias, J. Electrochem. Soc. 122, 59 (1975).

7. Surfanalyzer Model 150 System, Clevite Corp. Cleveland, Ohio.

NOMENCLATURE

d	glass wall width (mm)
F	location of virtual plane of focus (mm)
n_a	refractive-index of medium surrounding specimen (e.g., air)
n_f	refractive-index of fluid
n_g	refractive-index of glass walls
N	interferometric phase change (fringes)
p_r	optical path of a reflected ray (mm)
p_o	optical path of hypothetical unreflected ray (mm)
w	solid surface width (mm)
x	horizontal distance (mm)
x_f	x-coordinate of real plane of focus (mm)
x_B, y_B	position where a ray is reflected (mm)
y	vertical distance (mm)
y_D	position where a reflected ray leaves specimen (mm)
y_i	distance on an interferogram (mm)
λ	wavelength (nm)
ϕ_a	angle of reflected ray in surrounding medium (rad)
ϕ_f	angle of reflected ray in fluid (rad)
ϕ_g	angle of reflected ray in glass wall (rad)

FIGURE CAPTIONS

Fig. 1. Reflection from the rounded edge of a planar surface.

ABC incident ray reflected at point B

DBE surface tangent plane at point B

Fig. 2. Reflected ray trajectory.

ABCD reflected ray

GQE hypothetical unreflected ray

RQ virtual plane of focus

Q virtual origin of ray ABCD

DE equiphase arc centered on virtual origin Q

d glass wall thickness

w solid surface width

x_B position where ray is reflected

ϕ_a ray angle in surrounding medium

ϕ_f ray angle in fluid

ϕ_g ray angle in glass

F,S,T see text

Fig. 3. Electrode surface profiles.

a measured profile

b hyperbolic approximation $y = 0.00125/x$

Fig. 4. Electrode surface profiles.

a sharpest edge obtainable

b purposely rounded edge

Fig. 5. Calculated interferograms associated with reflection from the hyperbolic surface profile approximation shown in Fig. 3b.

——— n_f = 1.0000 (air)

- - - - n_f = 1.3340 (0.1 M $CuSO_4$)

A location of real plane of focus x_f = -0.5 mm

B x_f = 0

C x_f = 0.5 mm

D x_f = 1.0 mm

Fig. 6. Experimental interferograms of the interface between 0.1 M $CuSO_4$ and the electrode surface profile 3a. Designations as in in Fig. 5.

Fig. 7. Effect of edge curvature on experimental interferograms. Interface between air and the electrode surfaces shown in Fig. 4.

A x_f = 0, surface 4a

B x_f = 0, surface 4b

C x_f = 0.5 mm, surface 4a

D x_f = 0.5 mm, surface 4b

Fig. 8. Effect of aperture restriction on experimental interferograms. Interface between 0.1 M $CuSO_4$ and surface 3a.

A full (7.0°) aperture

B restricted (0.5°) aperture

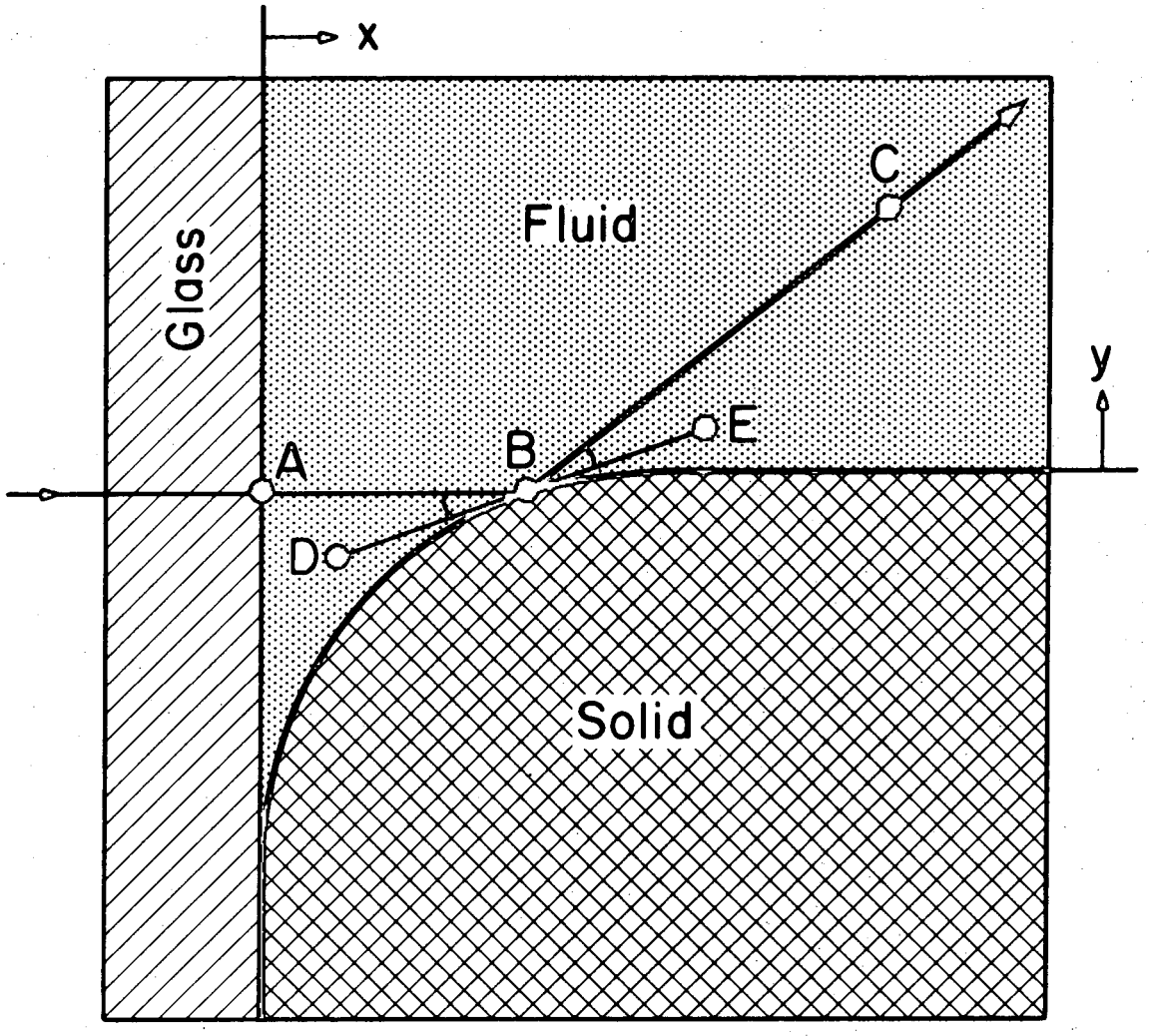

XBL 7311-4556

Fig. 1

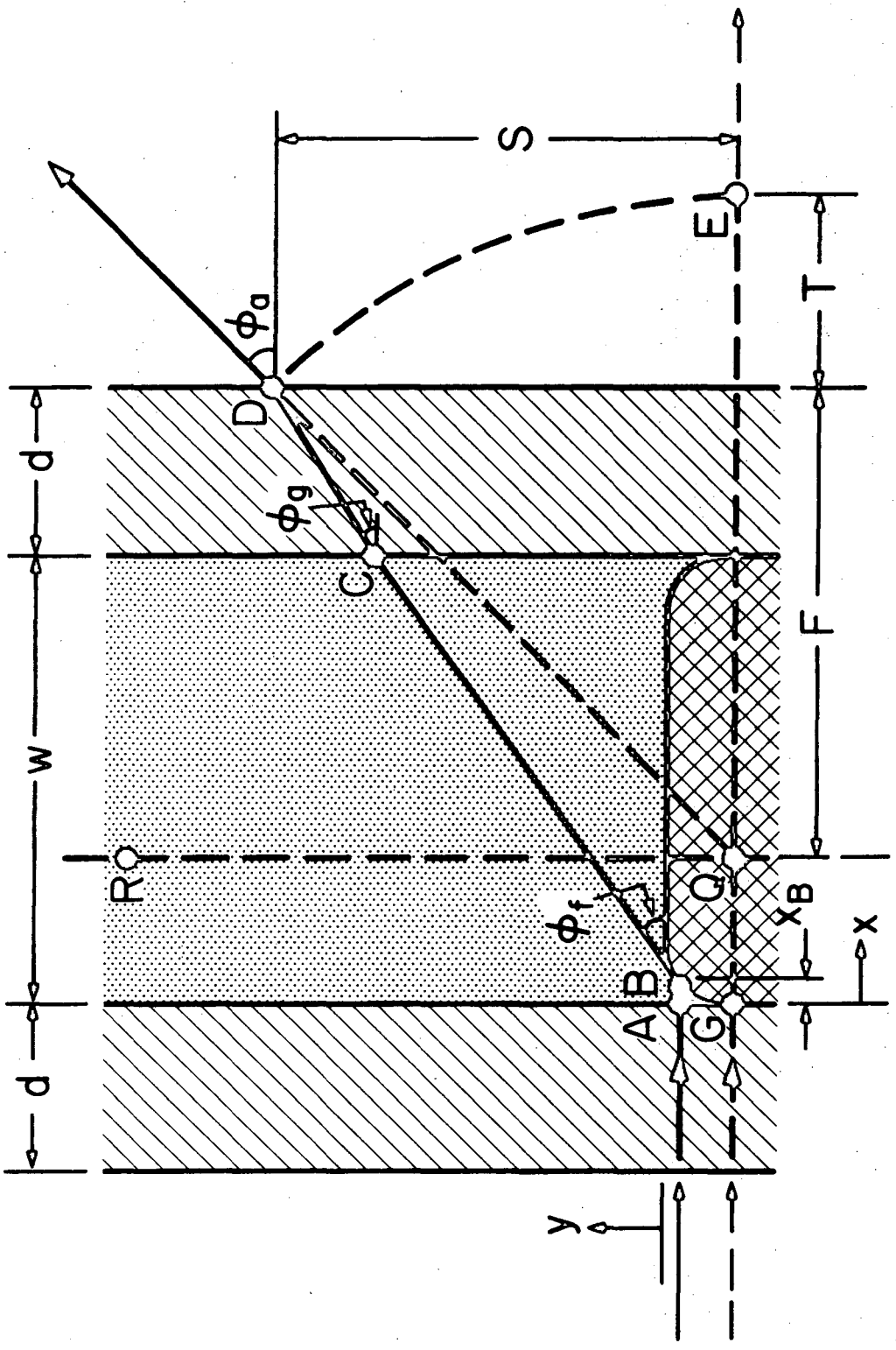

XBL748-4044

Fig. 2

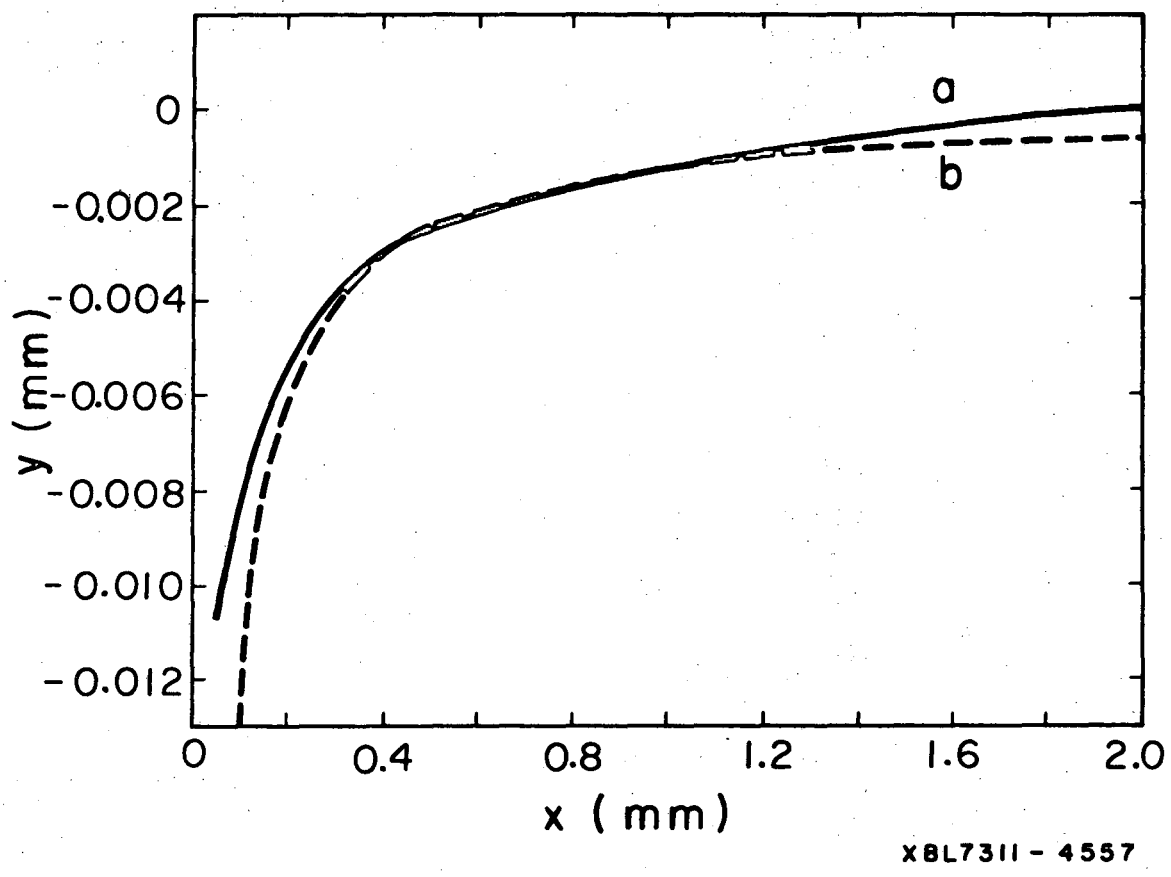
a
b
0
-0.002
-0.004
-0.006
-0.008
-0.010
-0.012
y (mm)
0
0.4
0.8
1.2
1.6
2.0
x (mm)
XBL7311-4557

Fig. 3

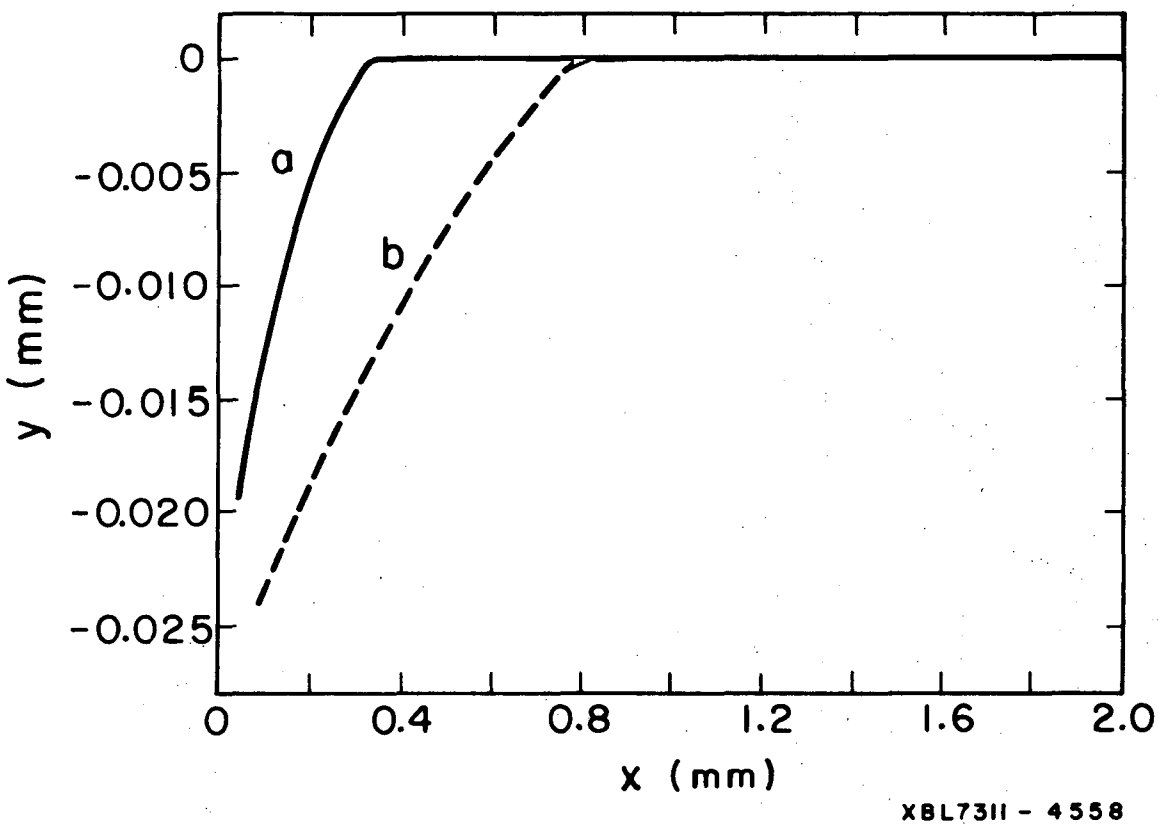
0
-0.005
-0.010
-0.015
-0.020
-0.025
y (mm)
a
b
0
0.4
0.8
1.2
1.6
2.0
x (mm)
XBL7311 - 4558

Fig. 4

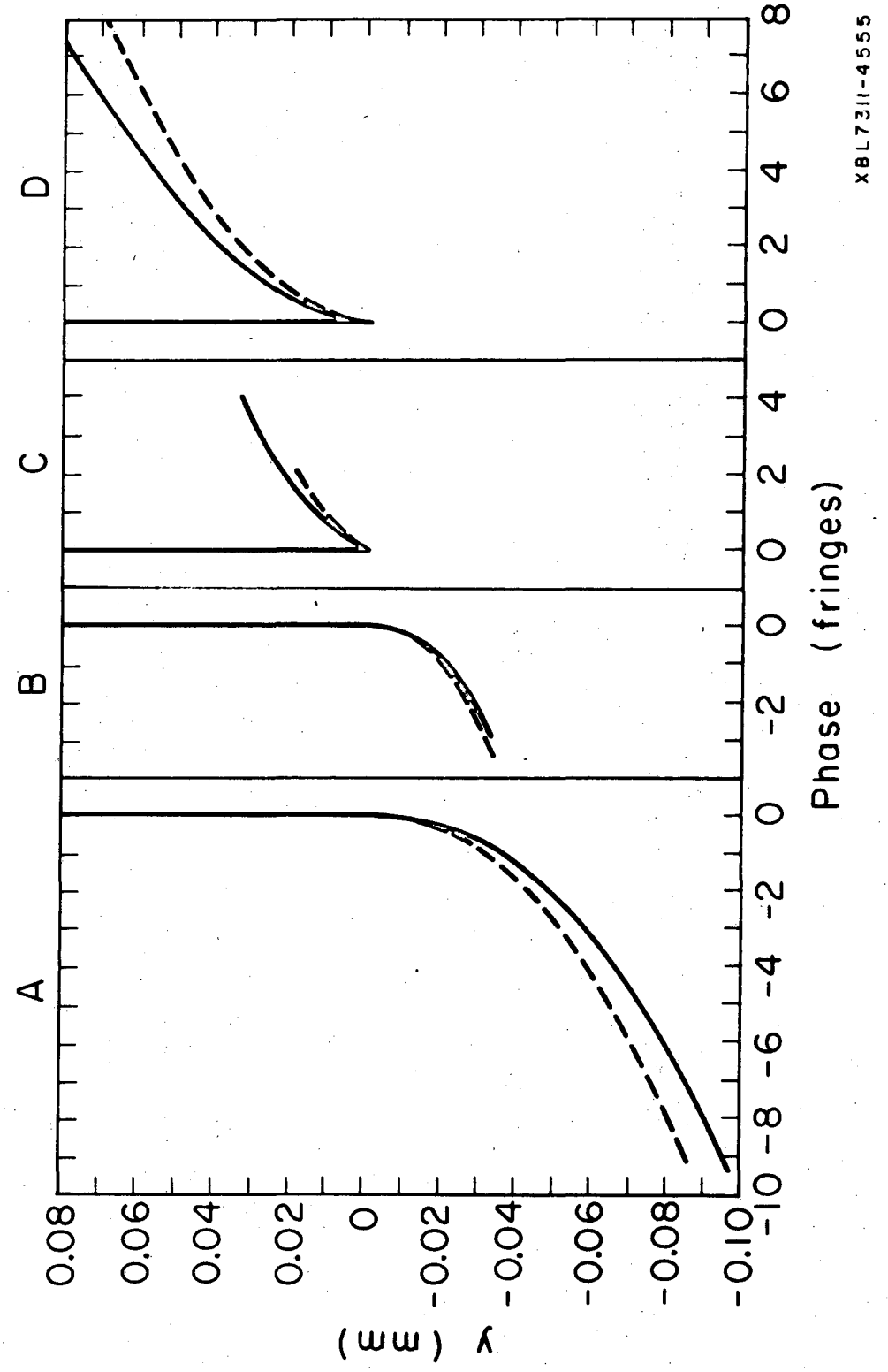
A
B
C
D
0.08
0.06
0.04
0.02
0
-0.02
-0.04
-0.06
-0.08
-0.10
y (mm)
-10 -8 -6 -4 -2 0 -2 0 2 4 0 2 4 6 8
Phase (fringes)
XBL7311-4555

Fig. 5

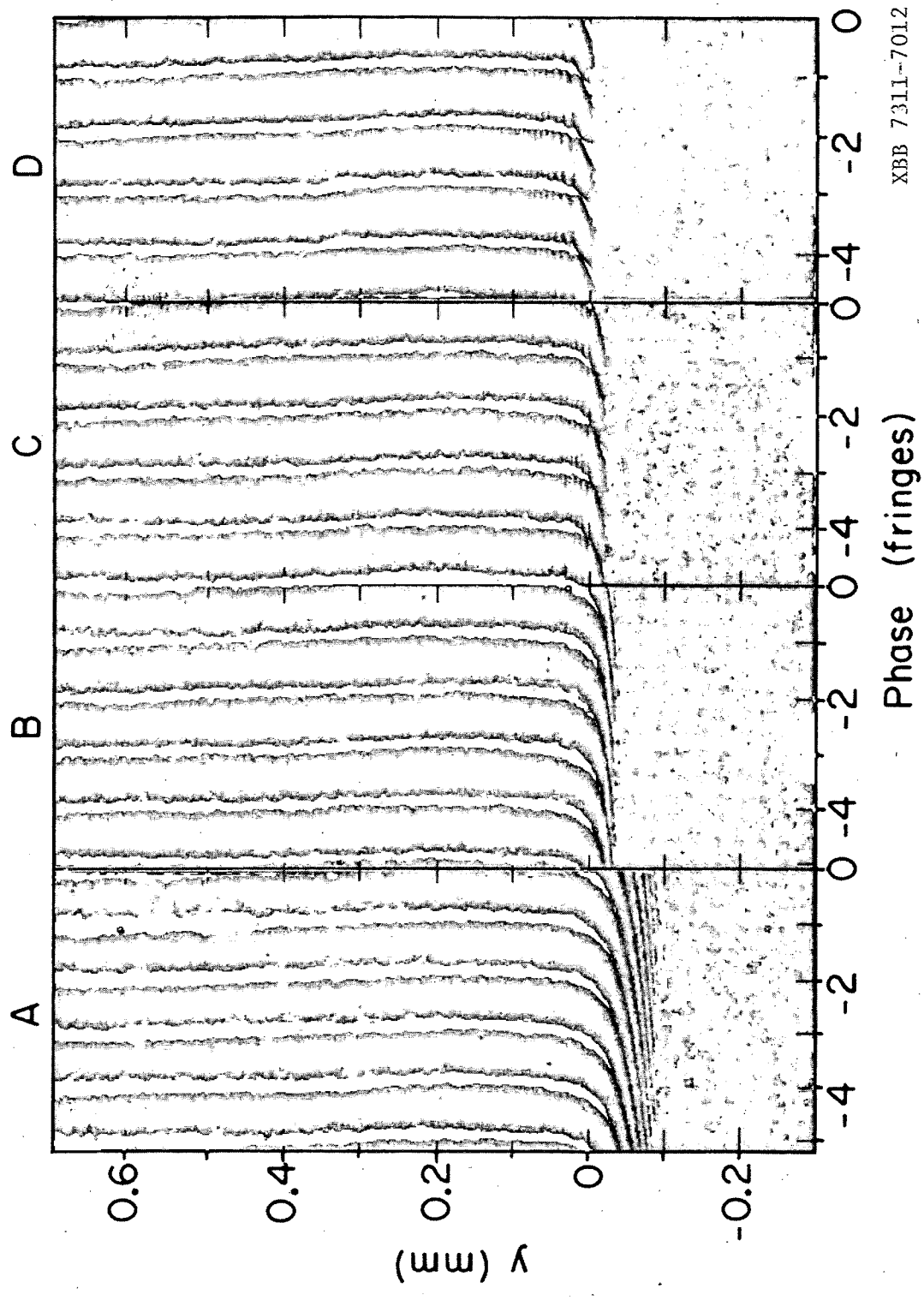
A
B
C
D
y (mm)
0.6
0.4
0.2
0
-0.2
-4
-2
0
-4
-2
0
-4
-2
0
-4
-2
0
Phase (fringes)
XBB 7311-7012

Fig. 6

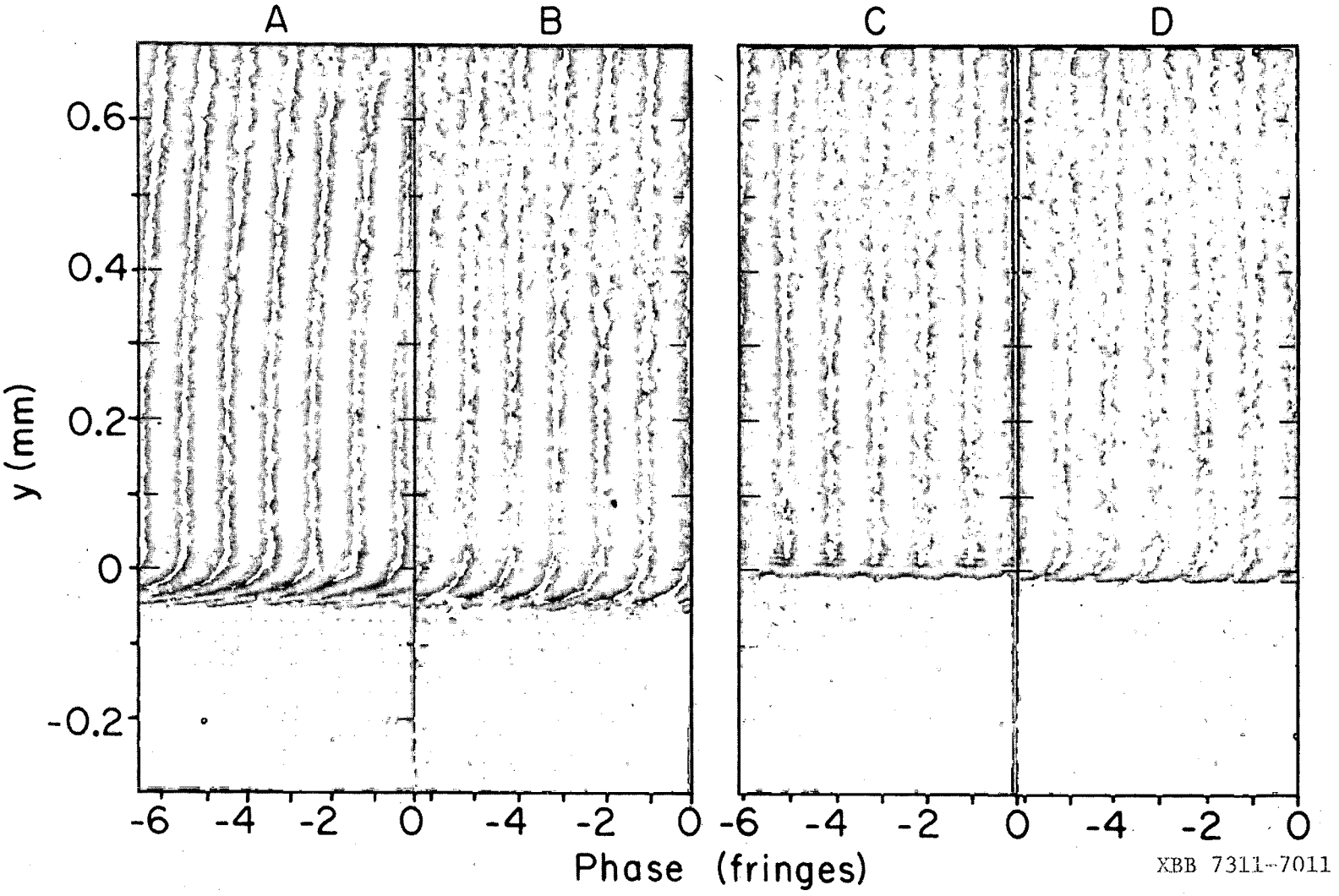

Fig. 7

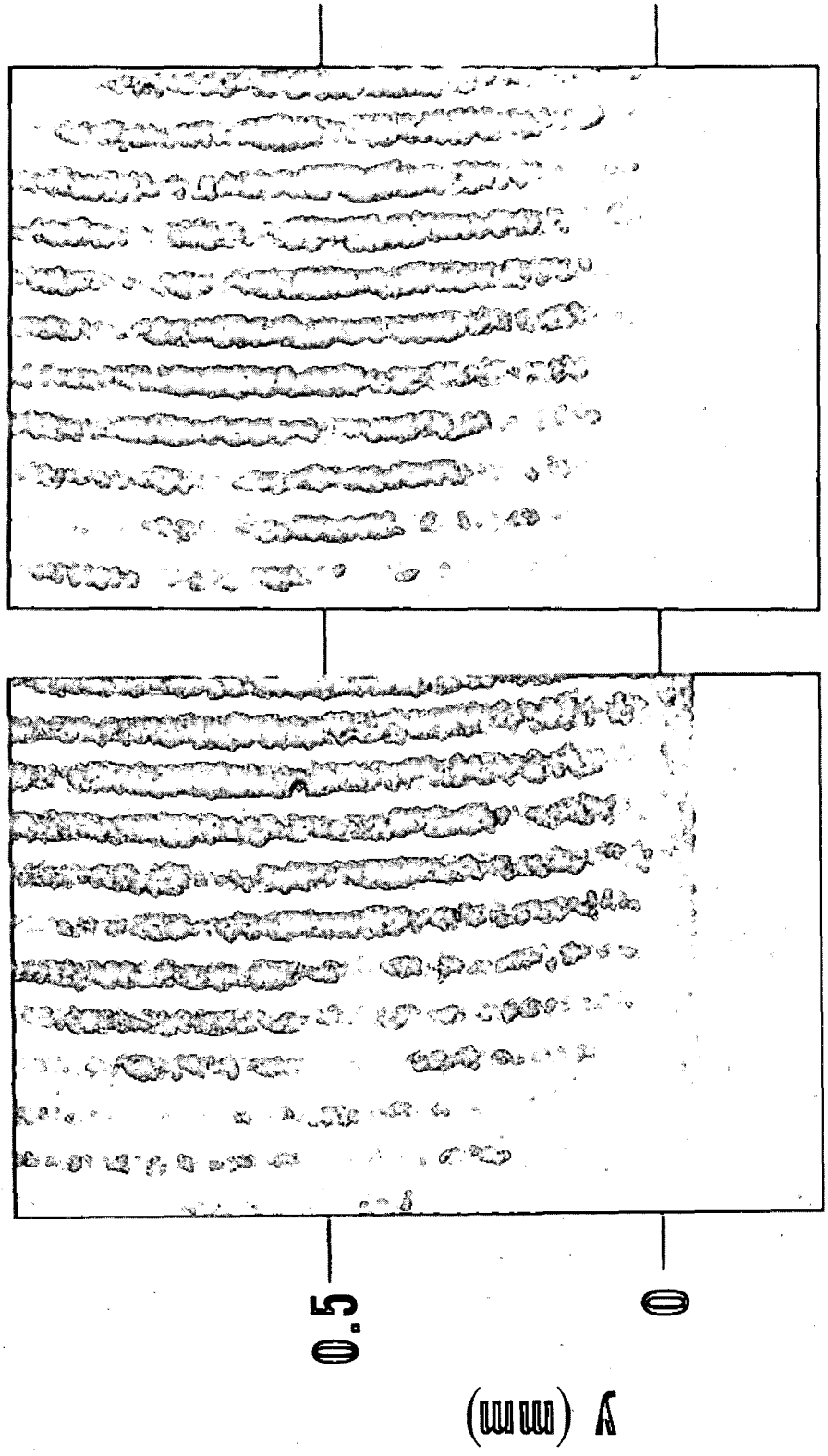

XBE 7411-8120

TECHNICAL INFORMATION DIVISION
LAWRENCE BERKELEY LABORATORY
UNIVERSITY OF CALIFORNIA
BERKELEY, CALIFORNIA 94720